Agglomeration and sintering in annealed FePt nanoparticle assemblies studied by small angle neutron scattering and x-ray diffraction

T. Thomson[1], S.L. Lee[2], M.F. Toney[3], C.D. Dewhurst[4], F.Y. Ogrin[5], C.J. Oates[2], S. Sun[6]

[1] Hitachi San Jose Research Center, 650 Harry Road, San Jose, CA 95120
[2] School of Physics and Astronomy, University of St. Andrews, St. Andrews, Fife KY16 9SS, UK
[3] Stanford Synchrotron Radiation Laboratory, Stanford Linear Accelerator Center, 2575 Sand Hill Rd, Menlo Park, CA 94025
[4] Institut Laue Langevin, 38042 Grenoble, France
[5] School of Physics, University of Exeter, Exeter EX4 4QL, UK.
[6] IBM – T.J.Watson Research Center, Yorktown Heights, NY 10598

Received: September 2004

PACS: 75.50.Tt, 61.12.Ex, 75.75.+a, 75.50.Bb

Abstract

In this work we give a detailed account of the use of small angle neutron scattering to study the properties of polymer mediated, self assembled nanoparticle arrays as a function of annealing temperature. The results from neutron scattering are compared with those obtained from x-ray diffraction. Both techniques show that particle size increases with annealing temperatures of 580°C and above. They also show that the distribution of particle diameters is significant and increases with annealing temperature. The complementary nature of the two measurements allows a comprehensive structural model of the assemblies to be developed in terms of particle sintering and agglomeration. To realise the potential of nanoparticle assemblies as a monodispersed data storage medium the problem of particle separation necessary to avoid sintering and agglomeration during annealing must be addressed.

I. INTRODUCTION

$L1_0$ phase, high magnetic anisotropy nanoparticles comprised of equiatomic FePt are attracting considerable attention[1-11] due to their potential in future nanomagnetic devices. Possible applications for magnetic nanoparticles in general include their use as permanent magnets,[2] biosensors,[12] biomedical applications[13] and drug delivery systems.[14] However, the initial work on high anisotropy nanoparticles has focused on their potential application as a data storage medium[15-20] with the ultimate goal of storing one data bit per particle giving an areal density of approximately 40Tbit/in^2. The high anisotropy found in bulk chemically ordered $L1_0$ materials[21] implies that nanoparticles with diameters of less than 3nm will have sufficient anisotropy to be magnetically stable at room temperature.

Work supported in part by the Department of Energy Contract DE-AC02-76SF00515

Solution-phase synthesis of nanoparticles has shown that particles with diameters of 4nm and very narrow size distributions (rms/mean = 0.05) can be produced.[1] These particles can then be deposited via self-assembly onto Si substrates as an ordered thin film array. The self-assembly technique allows good control over the arrangement of particles over lateral dimensions of microns. However, the as-deposited the particles are not in the chemically ordered, high anisotropy $L1_0$ phase and are typically observed to have only a small saturation magnetisation (M_s) and zero coercivity (H_c) at room temperature. In order to convert the as-deposited nanoparticles into the $L1_0$ phase it is necessary to anneal at temperatures above 500°C. Annealing at these temperatures allows the possibility of individual nanoparticles agglomerating to form larger particles. Other workers have recently reported that the temperature at which the onset of ordering occurs can be reduced through the use of dopants such as Cu,[22] Ag or Au.[23-24] Since one of the main attractions for nanoparticle arrays as a data storage medium is the monodisperse nature of the particles, we concentrate in this work on describing the interparticle changes that occur upon annealing arrays with three polymer mediated self-assembled layers deposited onto Si substrates. Comparing small angle neutron scattering (SANS) and x-ray diffraction (XRD) data allows a comprehensive structural model of unannealed nanoparticle arrays to be developed. We show that at the temperatures required to create the $L1_0$ phase, agglomeration always occurs in our samples and that the effect is more severe the higher the anneal temperature used. We conclude that in order to reach their full technological potential the problem of agglomeration and sintering during annealing must be addressed.

II. EXPERIMENTAL

FePt nanoparticles were prepared using a solution chemistry approach and deposited onto Si substrates polished on both sides using the polymer mediated, layer-by-layer technique described previously.[25-26] This resulted in films consisting of 3 layers of 4nm $Fe_{58}Pt_{42}$ self-assembled particles, this concentration having previously been shown to exhibit the highest coercivity.[1,26] The polymer-mediated approach results in nanoparticles with an extremely narrow size distribution, typically rms/mean <5%, and a well defined periodicity. The as-deposited films were annealed under nitrogen at atmospheric pressure over a range of temperatures from 580 to 800°C. All samples were annealed for 5mins except at the lowest temperature where they were annealed for 30mins. This difference in time is not critical at this temperature and so we treat this series of samples as an annealing temperature series.

A subset of the annealed films were studied using the D11 diffractometer[27] at the ILL in Grenoble, France using a neutron wavelength of $\lambda = 4.5$Å. The neutrons were collimated to give a beam diameter of 16mm. Data were collected at three detector positions in order to scan a $\mathbf{q}$ range of 0.012 – 0.3Å^{-1}. The small volume of material meant that it was necessary to stack a number of samples to increase signal to noise ratio. However,

counting times of several hours per detector position were still required to obtain statistically meaningful data.

X-ray diffraction data were collected at the National Synchrotron Light Source at the Brookhaven National Laboratory using beamline X20C. To reduce the background from the Si substrates, data were collected in a grazing incidence geometry. The diffracted beam was analyzed with 1 milliradian Soller slits, which provided a finer resolution than any of the diffraction peak widths. To calculate the grain size distribution of the FePt particles, the entire XRD data set was fitted to a model where the peak shapes contain contributions from non-uniform strain and grain size broadening.[28] The shape of each diffraction peak shape was then a convolution of the shapes due to grain-size broadening, which was assumed to originate from a lognormal distribution of grain sizes,[29-30] and to non-uniform strain, which was assumed to be Gaussian:

$$\mathrm{I(Q)} = \int_0^\infty \mathrm{P(Q}, d) \frac{\exp(\frac{-(d-d_0)^2}{2\sigma_d^2})}{\sqrt{2\pi\sigma_d}} \mathrm{d}d \qquad (1)$$

Here Q is the scattering vector, d is the plane spacing, d_0 is the average plane spacing, σ_d is the root-mean-square width of the Gaussian d-spacing distribution, and P(Q, d) is the shape for a lognormal distribution of grain sizes (Eqns. (6) and (15) in Ref. [30] with Q = 2πs). For simplicity, the lognormal width (σ_d) was fixed at 0.5. In all cases, when σ_d was allowed to vary, it converged to a value close to 0.5.

In a binary alloy, such as FePt, the extent of chemical order is quantified by the Warren long-range order parameter:

$$S = r_{Fe} + r_{Pt} - 1 = \frac{(r_{Pt} - x_{Pt})}{y_{Fe}} = \frac{(r_{Fe} - x_{Fe})}{y_{Pt}} \qquad (2)$$

Here x_{Pt} and x_{Fe} are the atom factions of Fe and Pt, respectively r_{Fe} and r_{Pt} are the fraction Fe and Pt sites occupied by the correct atom in the $L1_0$ structure; and y_{Pt} and y_{Fe} are the fraction of correct Fe and Pt sites, 0.5 in for the $L1_0$ phase (see Cebollada[31] or Warren[28] for details). When the chemical order is perfect, each alternating layer perpendicular to the c axis is fully occupied by Fe or Pt atoms (i.e., all the Fe sites are occupied by Fe atoms and Pt sites by Pt atoms) and S=1. For complete chemical disorder, all sites are equally occupied by Fe and Pt and S=0. For partial chemical order, S is proportional to the number of atoms on correct sites $(r_{Fe} + r_{Pt})$. The discussion above is applicable to homogeneous materials, but a material can be inhomogeneous, consisting of regions that have high chemical order and regions that are nearly disordered (e.g., a two-phase system). This distinction between the microstructures suggests that an additional factor is needed to quantify chemical order in inhomogeneous materials. This is the volume fraction of the film that is chemically ordered, which we call f_0. For inhomogeneous materials, we can then distinguish and measure f_0, S_{order} (S in the

chemically ordered regions), and S_{ave} (the volume averaged S). This is important because the nanoparticle assemblies (as with thin films[32]) are, in fact, inhomogeneous.

In order to calculate S_{order}, f_0, and S_{ave}, we use the ratio of the integrated intensities of the various diffraction peaks corrected for the Lorentz-polarization factor, illuminated area and the Debye-Waller parameter.[28,33-34] S_{order} is calculated from the ratio of these corrected integrated intensities of the $L1_0$ (110) and (220) peaks. The ordered fraction, f_0, is determined from the fitted intensities of the fcc(220) and $L1_0$ (202) and (220) peaks; f_0 is the ratio of the $L1_0$ peaks to the sum of the three peak intensities. The average chemical order S_{ave} is the product of S_{order} and f_0. As a check and to improve the accuracy of the analysis, S_{ave} was also determined from the ratio of the $L1_0$ (110) peak to the sum of the fcc(220) and $L1_0$ (202) and (220) peaks. An explicit, detailed discussion of this procedure is given in Cebollada[31].

III. SIMULATIONS OF SANS DATA

In principle, small angle neutron scattering gives information on both nuclear and magnetic scattering potentials. The nuclear and magnetic contributions sum to give the total measured intensity as a function of scattering vector $\mathbf{q}$ where $|\mathbf{q}| = 4\pi \sin(\theta)/\lambda$ and for the case of a magnetically saturated sample the intensity is given by [35-36]

$$I(\mathbf{q}) = I_N(\hat{\mathbf{q}}) + \left(1 - (\hat{\mathbf{h}}.\mathbf{q})^2\right) I_M(\mathbf{q}) \qquad (3)$$

where $\hat{\mathbf{h}}$ is a unit vector in the direction of the magnetization, and $I_N(\mathbf{q})$ and $I_M(\mathbf{q})$ depend on the q-dependent nuclear and magnetic scattering cross-sections.

For simplicity we consider a distributed set of particles each at positions $\mathbf{r}_i$ having a scattering potential $U(\mathbf{r} - \mathbf{r}_i)$. For nuclear scattering this is the nuclear scattering potential $U_N(\mathbf{r} - \mathbf{r}_i)$ due to the residual strong interaction of the neutron with the nucleus, while for magnetic scattering this is the magnetic dipolar interaction $U_M(\mathbf{r} - \mathbf{r}_i)$ between the neutron and the local spatially varying magnetic flux density due to the magnetic particle.

The contribution to the total intensity of each depends on the partial differential cross-section $\frac{d\sigma}{d\Omega}$ for each interaction, which is the number of neutrons scattered per second into unit solid angle, divided by the incident neutron flux. Primary data reduction includes a step which normalizes the scattering data to the incident flux and hence to extract information from our scattering results we simulate $\frac{d\sigma}{d\Omega}(\mathbf{q})$. The partial differential cross-section for a system of volume V, containing N_p particles where each particle contains many individual (either nuclear or magnetic) scattering centers can be written as [37-38]:

$$\frac{d\sigma}{d\Omega}(\mathbf{q}) = \frac{1}{V}\left\langle \sum_{i=1}^{N_p}\sum_{i'=1}^{N_p} F_i(\mathbf{q})F_{i'}^*(\mathbf{q})e^{-i\mathbf{q}\bullet(\mathbf{r}_i-\mathbf{r}_{i'})} \right\rangle \tag{4}$$

where the brackets indicate an average over the ensemble. The quantity

$$F_i(\mathbf{q}) = c\int \mathrm{U}_i\, e^{-i\mathbf{q}\bullet\mathbf{r}} d^3\mathbf{r} \tag{5}$$

often referred to as the *form factor*, is the Fourier transform of the local scattering potential, U_i, due to particles at $\mathbf{r}_i$, where the constant c depends on the nature of the interaction. We note that in the case of scattering of a spherically symmetric potential the Born approximation allows the form factor to be written as $F_i(\mathbf{q}) = \int \mathrm{b}_i\, e^{-i\mathbf{q}\bullet\mathbf{r}} d^3\mathbf{r}$ where the scattering length b_i is defined by $\int_{particle} U_i(\mathbf{r})d\mathbf{r} = \frac{2\pi\hbar^2}{m} b_i$.

We next separate scattering into intraparticle i = i' and interparticle i ≠ i' contributions. For intra-particle scattering equation (4) gives

$$i = i' \colon \frac{\mathrm{d}\sigma}{\mathrm{d}\Omega}(\mathbf{q}) = \frac{N_p}{V}\left\langle F^2(\mathbf{q})\right\rangle. \tag{6}$$

In deriving the inter-particle terms we consider a system in which there is no correlation between the values of the scattering potentials (e.g. particle size and/or orientation) and their positions. This is a reasonable assumption for self-assembled FePt nanoparticles with a relatively low packing fraction. Thus the interference term may be factorized as:

$$i \neq i' \colon \frac{d\sigma}{d\Omega}(\mathbf{q}) = \frac{1}{V}\sum_{\substack{i=1 \\ i\neq i'}}^{N_p}\sum_{i'=1}^{N_p}\left\langle F_i(\mathbf{q})\right\rangle\left\langle F_{i'}^*(\mathbf{q})\right\rangle\left\langle e^{-i\mathbf{q}\bullet(\mathbf{r}_i-\mathbf{r}_{i'})}\right\rangle \tag{7}$$

which leads to

$$i \neq i' \colon \frac{d\sigma}{d\Omega}(\mathbf{q}) = \frac{N_p}{V}\left\langle F(\mathbf{q})\right\rangle^2 H(\mathbf{q}) \tag{8}$$

where the pair correlation function is defined as

$$H(\mathbf{q}) = \frac{1}{N_p}\sum_{\substack{i=1 \\ i\neq i'}}^{N_p}\sum_{i'=1}^{N_p}\left\langle e^{-i\mathbf{q}\bullet(\mathbf{r}_i-\mathbf{r}_{i'})}\right\rangle \quad . \tag{9}$$

Combining these two cases into a single expression gives

$$\frac{d\sigma}{d\Omega}(\mathbf{q}) = \rho\left\langle F(\mathbf{q})^2\right\rangle + \rho\left\langle F(\mathbf{q})\right\rangle^2 H(\mathbf{q}) \tag{10}$$

where the number density of the particles is defined as $\rho = \frac{N_p}{V}$.

The structure factor S(**q**) is related to the pair correlation function though $S(\mathbf{q}) = 1 + H(\mathbf{q})$, where $S(\mathbf{q}) = \frac{1}{N_p}\sum_{i}^{N_p}\sum_{i'}^{N_p}\left\langle e^{-i\mathbf{q}\bullet(\mathbf{r}_i - \mathbf{r}_{i'})}\right\rangle$ and the double summation runs over all i ,i'.

Thus the scattering cross-section can be written in terms of the structure factor as

$$\frac{d\sigma}{d\Omega}(\mathbf{q}) = \rho\left\langle F(\mathbf{q})\right\rangle^2 S(\mathbf{q}) + \rho\left(\left\langle F^2(\mathbf{q})\right\rangle - \left\langle F(\mathbf{q})\right\rangle^2\right) \tag{11}$$

For amorphous arrangements of particles $S(\mathbf{q})$ is well represented by the Percus-Yevick formula for interacting hard spheres,[39] and describes the interference effects of scattering from different particles. This contains information about the local arrangement of particles relative to one another. The **second** term in (11) is effectively the correction to the first term of (10) to account for the fact that all particles in the system are not identical. For a set of identical particles equations (10) and (11) become:

$$\frac{d\sigma}{d\Omega} = \rho\left\langle F(\mathbf{q})\right\rangle^2 S(\mathbf{q}) \tag{12}$$

We now have a formalism for a dispersion of identical particles that includes the effects of interparticle interference. In the literature (11) and (12) are frequently used to describe scattering from polydispersed and monodispersed systems of particles respectively. In order to obtain a realistic model of the nanoparticle arrays the effects of a distribution of particles sizes must be included, and proper account should be taken of the interference terms. In terms of a distribution of particle sizes $f(\sigma_m)$ of radius σ_m the differential cross-section (11) can be written as [40-41]:

$$\frac{d\sigma}{d\Omega} = \rho\int_0^\infty F_m^2(q) f(\sigma_m) d\sigma_m + \rho\int_0^\infty\int_0^\infty F_m(q) F_n(q) H_{mn}(q) f(\sigma_m) f(\sigma_n) d\sigma_m d\sigma_n \,. \tag{13}$$

While for systems that are close to being monodispersed, (10), (11) and (12) are all reasonable approximations,[41] as the systems become more polydispersed it becomes necessary to properly account for the interparticle interference terms via (13). This is the

approach we have used in this work. Even for the case of high polydispersity, in a densely packed system the use of (12) over (13) can lead to significant errors in simulating the data, since undue weight is given to particles of larger diameter. This problem has been solved analytically in the Percus-Yevick approximation for the case of a particle size distribution give by a Schulz (gamma) distribution of diameters by Griffith et al.[41] using (13) as a starting point. The Schulz (gamma) distribution is given by

$$f(\sigma) = \frac{\sigma^{c-1}\exp(-\sigma/b)}{b^c\,\Gamma(c)} \qquad (14)$$

where $b = \sigma_{mean}/(z+1)$

$c = z+1$

and z is the Schultz distribution width factor (z > -1). The Schulz (gamma) distribution is chosen due to its mathematical tractability. However, the distribution has a functional form similar to that of a log-normal distribution and is therefore physically very reasonable to describe to describe an assembly of particles.

We first consider the contribution from magnetic scattering. Since a field greater than 2 Tesla is required to saturate our FePt nanoparticle assemblies it was not possible during the SANS experiments to align the particles magnetically. In zero applied magnetic field, for a random distribution in 3D of magnetisation directions, the magnetic contribution to scattering depends is equal along all directions $\mathbf{q}$ and is proportional to $\frac{1}{3}\langle M^2(\mathbf{q})\rangle$, where $\langle M(\mathbf{q})\rangle = \left\langle \int M(\mathbf{r}) e^{-i\mathbf{q}\bullet\mathbf{r}} d^3\mathbf{r} \right\rangle$ is the average value of the Fourier component of the local spatially varying magnetization $M(\mathbf{r})$, analogous to the form factor $F(\mathbf{q})$ in the foregoing discussion. In order to separate out the magnetic contribution from the nuclear scattering, one can use the anisotropic contribution to the scattering due to the total or partial polarization of the magnetization, as indicated in (3). The magnetic scattering is suppressed along the direction in which the magnetization lies; for the case of a saturated magnetic sample, the magnetic scattering goes to zero along the direction of the applied magnetic field. We have used this technique to successfully extract the magnetic scattering from the thin films of continuous longitudinal recording media, where the grains diameters and film thickness are of similar dimensions to the FePt nanoparticle system considered here[42]. In the present work we attempted to evaluate the size of the magnetic signal relative to the nuclear scattering using the same approach. For applied fields of up to 1.3T the anisotropic magnetic signal was not apparent in these samples, implying that even in zero field the scattering is dominated by the nuclear scattering due to the strong contrast in neutron scattering potential between the metallic particles and the organic matrix in which they are embedded. In the analysis which follows we assume that the scattering originates entirely from the nuclear cross-section. In reality, since we are making all measurement in zero field on samples in the virgin magnetic state, and given that at these particle sizes the magnetic grain size is likely to closely resemble the

physical grain size, then in modeling the dispersion of particle sizes such an assumption is not likely to unduly prejudice the distributions we obtain from the analysis.

Using Griffith's[41] analytic solution to (13) allowed an extensive series of simulations to be undertaken to investigate the effect of the various parameters on the simulated data. These simulation experiments showed that the interference term was relatively unimportant in determining the **q** dependence of the scattering intensity for the particle concentration in the assemblies investigated here where the volume fraction is 0.13.[39] Attempts to simulate the experimental data using a single Schulz (gamma) distribution produced a reasonable fit to the data. However, the refinement of including a second distribution function improved the quality of the fit, and since for wide distributions incoherent scattering strongly reduces the relative contribution of the particle-particle inference term, this refinement does not introduce significant errors. The error bars on the data sets are such that some small changes in the functional form of the particle diameter distribution function to do not affect the quality of the fit provided that the median particle diameter and the distribution width remain the same. Thus whilst the exact form of the particle diameter distribution is subject to some small uncertainties the overall functional form can be accurately simulated. In order to check the validity of the simulations a similar polydisperse model of interacting particles proposed by Kotlarchyk et al.[37] was tested. Simulations using this model produced very similar results to the Griffith model showing that simulations of the SANS data are not model dependent. Also attempted were simulations using just a distribution of hard sphere diameters. This also produced similar parameters as fits to the Griffith model showing that, particularly for wide distributions, the interference terms do not contribute significantly to the form of total scattered intensity.

IIII. RESULTS AND DISCUSSION

Fig.1a shows a scanning electron microscope (SEM) image of an as-deposited nanoparticle assembly. Fig.1b is an image of the SANS detector (64 x 64 element) showing the data with the normal instrumentation corrections. It is immediately apparent that there is significant coherent scattering from the particles giving rise to the observed ring. The interference terms in the scattering leads to a S(q) which cause the scattering intensity to peak at $|q| \sim \frac{2\pi}{d}$, where d is the nearest neighbor separation. An estimate of the position of this peak was obtained by azimuthally integrating around the detector and fitting to a Gaussian function. This yielded a peak at $|q| \approx 0.1\text{Å}^{-1}$ corresponding to a nanoparticle plane spacing, d, of 6.4nm, in excellent agreement with the particle periodicity found from TEM and SEM images.[25] The fact that the scattering involves a S(q), with a width equivalent to 1.2nm in real space, rather than sharp Bragg peaks indicates that long range order does not extend over the entire coherence length of the neutrons. The lack of long range orientational order is also indicated by the fact that peak intensity is evenly distributed around a ring on the detector. This absence of both spatial and orientational order over large areas is clearly a limitation of self-assembled arrays which might be addressed by depositing the nanoparticles onto pre-patterned substrates such that the perfectly ordered arrays are only required over a few microns. These data

were analysed in more detail using the Griffith model where a particle diameter of 4.0nm was obtained assuming a packing fraction of 0.13 and a particle separation of 6.5 nm, in agreement with the simple analysis presented above. These values are also consistent with results obtained on similar particle assemblies studied using SEM and TEM where particle diameters of 4 nm with a narrow distribution of sizes were observed.[1] In contrast, performing a detailed analysis of the Bragg peaks in the XRD data, as described above, a crystallographic, volume averaged particle diameter of 2.2 nm is obtained.[43] These differences can be explained by considering the different physical effects being probed. XRD is sensitive to coherent planes of atoms *within the particle* whereas SANS is sensitive only to particle sizes, shapes and *interparticle* correlations, and SEM/TEM requires a large electron scattering contrast. Hence combining the different sensitivities of SANS and XRD allows a more complete physical description of these nanoparticle systems than either technique could provide in isolation. The data suggest a model where particles consist of a well defined metallic core surrounded by a shell of amorphous material. This model is also strongly supported by magnetisation and NEXAFS data.[43,44] Measurements of magnetisation vs. applied field as a function of temperature show that the unannealed arrays are superparamagnetic and that the data are well described by a Langevin function where the saturation magnetisation is 1030 emu/cm^3, which is the value for disordered fcc FePt, and a particle diameter of 2.2 nm. NEXAFS results show that the as-deposited particles have very little spectral intensity due to Fe in a metallic environment and that the observed signal can be modeled as originating from Fe oxide. Due to the escape depth of secondary electrons the atoms at the surface of a particle are largely responsible for the observed signal as discussed in detail by Anders et al.[44] Hence we are now able to understand the physical state of the unannealed nanoparticles in terms of a metallic, magnetically active core of diameter 2.2nm surrounded by a non, or only very weakly magnetic, shell. This model of as-deposited nanoparticle arrays will then act as starting point in order to understand the annealing process.

In order to investigate the evolution of nanoparticle assemblies with annealing we have measured the magnetic and structural properties as a function of annealing temperature. Changes in magnetic properties have already been reported[43] and here we concentrate on structural aspects. Fig.2 shows SANS data and simulations, which include a small constant background term, together with the distributions of particle diameters used to produce the simulations, as a function of annealing temperature. In the case of the sample annealed under the 700°C/5min condition the particle diameters had increased to a size which gave scattering at a q lower than that accessible experimentally. Hence for this sample the distribution of diameters obtained from simulations of the data sets a lower bound on the particle size distribution, rather than providing full information on the distribution. The limit of the data is marked on the fig.2. Also shown are the distributions of particle diameters determined from XRD measurements using the analysis method described above. These data are summarized in fig.3 where the median diameters and width of the particle size distributions are plotted. These results immediately show that even at the lowest anneal temperature required to produce significant coercivity at room temperature we observe both agglomeration and sintering. The two techniques also demonstrate a significant distribution of particles sizes with the SANS data giving a tail of large diameter particles for the 580°C/30min anneal condition. At higher annealing

temperatures the distribution of diameters and the median diameter obtained from the SANS measurement increases rapidly. The particle diameters obtained from the x-ray analysis also increase substantially. Since the width of the x-ray peaks forms the basis of the particle size analysis, it follows that the x-ray measurement is sensitive only to coherent lattice planes. Hence annealing the particles results in a x-ray diameter greater than the initial particle size and we associate the increased diameter with particle sintering where particles combine to form a larger entity with a common crystallographic axis.

Fig.4 shows $L1_0$ ordering in these particles. As mentioned in the previous section it is important to note that, in common with many $L1_0$ materials, the chemical ordering in the nanoparticles is inhomogeneous: there are regions that are chemically ordered and those that are chemically disordered. The extent of order within the ordered regions is shown by the squares, whilst the fraction of the assembly that is chemically ordered is shown by the circles. With this in mind, the data in fig.4 demonstrate that chemical ordering in particle assemblies has two components. Firstly the degree of ordering within the population of particles that are ordered, shows that such particles are close to being fully ordered. The fraction of particles that are ordered increases from 60% for the 580°C/30min anneal condition to 90% for the 800°C/5min treatment, a commensurate increase in coercivity (measured at T = 20K) from 9.8kOe to 36.9kOe has also been found.[43] Thus even after annealing at the highest temperature for 5 mins, not all particles are chemically ordered despite the fact that severe agglomeration has already occurred. These results on ordered fractions show a potentially severe limitation since any high density recording scheme is likely to demand a medium that has uniform properties.

V. CONCLUSION

We have demonstrated the utility of combining SANS measurements with XRD to gain an understanding of the physical structure of nanoparticle assemblies. In this way we are able to separate the effects of particle sintering from those of agglomeration. We provide evidence that unannealed particles consist of a metallic, magnetic core surrounded by an oxide containing shell, consistent with magnetization data reported previously.[43] The data show that annealing leads to a large change in the median particle size and that a large distribution of particle sizes exists. The data also provide evidence that to first order the macroscopic magnetic properties of the assemblies are not dependent on the particle sizes but depend instead on the fraction of particles with $L1_0$ ordering, f_o. The work clearly demonstrates that if nanoparticle arrays are to become a viable recording technology where data is stored on one bit per particle then the problem of particle sintering and agglomeration must be addressed. However the promise of storage densities above 1 Tbit/in^2 provides a strong incentive for future research in FePt nanoparticles and ensures that this will continue to be an active area of endeavor.

Acknowledgements

This research was carried out in part at the National Synchrotron Light Source, Brookhaven National Laboratory, which is supported by the U.S. Department of Energy, Division of Materials Sciences and Division of Chemical Sciences, under Contract No. DE-AC02-98CH10886. Portions of this research were carried out at the Stanford Synchrotron Radiation Laboratory, a user facility operated by Stanford University on behalf of the U.S. Department of Energy, Office of Basic Energy Sciences.

References

[1]S. Sun, C. B. Murray, D. Weller, L. Folks and A. Moser, Science **287**, 1989 (2000).

[2]H. Zeng, J. Li, J. P. Liu, Z. L. Wang and S. Sun, Nature **420**, 395 (2002).

[3]Q.A. Pankhurst, J. Connolly, S.K. Jones and J. Dobson, J. Phys. D: Appl. Phys. **36**, R167 (2003).

[4]S. Kang, J. W. Harrell and D. E. Nikles, Nanolett. **2**, 1033 (2002).

[5]S. Stappert, B. Rellinghaus, M. Acet and E. F. Wassermann, J. Cryst. Growth **252**, 440 (2003).

[6]T. Hyeon, Chem. Comm. **8**, 927 (2003).

[7]B. Jeyadevan, K. Urakawa, A. Hobo, N. Chinnasamy, K. Shinoda, K. Tohji, D. D. J. Djayaprawira, M. Tsunoda and M. Takahashi, Jap. J. Appl. Phys. Part 2 Lett. **42**, L350 (2003).

[8]Y. Huang, H. Okumura, G. C. Hadjipanayis and D. Weller, J. Magn. Magn. Mater. **242**, 317 (2002).

[9]T. J. Klemmer, N. Shukla, C. Liu, X. W. Wu, E. B. Svedberg, O. Mryasov, R. W. Chantrell, D. Weller, M. Tanase and D. E. Laughlin, Appl. Phys. Lett. **81**, 2220 (2002).

[10]Z. R. Dai, S. Sun and Z. L. Wang, Surface. Sci. **505**, 325 (2002).

[11]B. Stahl, J. Ellrich, R. Theissmann, M. Ghafari, S. Bhattacharya, H. Hahn, N. S. Gajbhiye, D. Kramer, R. N. Viswanath, J. Weissmüller and H. Gleiter, Phys. Rev. B **67**, 014422 (2003).

[12]G. V. Kurlyandskaya, M. L. Sanchez, B. Hernando, V. M. Prida, P. Gorria and M. Tejedor, Appl. Phys. Lett. **82**, 3053 (2003).

[13]D. K. Kim, M. Mikhaylova, Y. Zhang, M. Muhammed, Chem. Mater. **15** 1617 (2003).

[14]F. Scherer, M. Anton, U. Schillinger, J. Henkel, C. Bergemann, A. Kruger, B. Gansbacher and C. Plank, Gene Therapy **9**, 102 (2002).

[15]S. Sun, D. Weller and C.B. Murray, in *The Physics of Ultra-High-Density Magnetic Recording* edited by M. L. Plumer, J. van Ek and D. Weller (Springer, New York, 2001).

[16]S. Anders, M. F. Toney, T. Thomson, J.-U. Thiele, B. D. Terris, S. Sun and C. B. Murray, J. Appl. Phys. **93**, 6299 (2003).

[17]J.W. Harrell, S. Wang, D.E. Nikles and M. Chen, Appl. Phys. Lett. **79**, 4393 (2001).

[18]X.W. Wu, K.Y. Guslienko, R.W. Chantrell and D. Weller, Appl. Phys. Lett. **82**, 3475 (2003).

[19]R. W. Chantrell, D. Weller, T. J. Klemmer, S. Sun and E. E. Fullerton, J. Appl. Phys. **91**, 6866 (2002).

[20]E. Mayes, A. Bewick, D. Gleeson, J. Hoinville, R. Jones, O. Kasyutich, A. Nartowski, B. Warne, J. Wiggins and K.K.W. Wong, IEEE Trans. Magn. **39**, 624 (2003).

[21]D. Weller and A. Moser, IEEE Trans. Magn. **35**, 4423 (1999).

[22]X. Sun, S. Kang, J.W. Harrell, D.E. Nikles, Z.R. Dai, J. Li and Z.L. Wang, J. Appl. Phys. **93**, 7337 (2003).

[23]S.S. Kang, D.E. Nikles and J.W. Harrell, J. Appl. Phys. **93**, 7178 (2003).

[24]J.W. Harrell private comm.

[25]S. Sun, S. Anders, H. Hamann, J.-U. Thiele, J. E. E. Baglin, T. Thomson, E. E. Fullerton, C. B. Murray and B. D. Terris, J. Am. Chem. Soc. **124**, 2884 (2002).

[26]S. Sun, S. Anders, T. Thomson, J. E. E. Baglin, M. F. Toney, H. Hamann, C. B. Murray and B. D. Terris, J. Phys. Chem. B. **107**, 5419 (2003).

[27]P. Lindner, R.P. May and P.A. Timmins, Physica B **180 & 181**, 967 (1992).

[28]B.E. Warren, *X-Ray Diffraction* (Dover, Reading MA, 1969).

[29]W.L. Prater, E.L. Allen, W-Y. Lee, M.F. Toney, J. Daniels and J.A. Hedstrom, Appl. Phys. Lett. **84**, 2518 (2004).

[30]N.C. Poppa and D. Balzar, J. Appl. Crystallogr. **35**, 338 (2002).

[31]A. Cebollada, R. F. C. Farrow, M. F. Toney, in *Magnetic Nanostructures*, edited by H. S. Nalva (American Scientific Publishers, Stevenson Ranch, 2002), p. 93.

[32]M.F. Toney, W.Y. Lee, J.A. Hedstrom and A. Kellock, J. Appl. Phys. **93**, 9902 (2003).

[33]R.F.C. Farrow, D. Weller, R.F. Marks, M.F. Toney, S. Hom, G.R. Harp and A. Cebollada, Appl. Phys. Lett. **69,** 1166 (1996).

[34]M.F. Toney and D.G. Wiesler, Acta Crystallographica A **49**, 624 (1993).

[35]D.J. Cebula, S.W. Charles and J. Popplewell, Colloid and Polymer Sci. **259**, 395 (1981).

[36]G. Kostorz, in *Treatise on Materials Science and Technology Vol. 15: Neutron Scattering* edited by G. Kostorz (Academic Press, New York, 1979).

[37]M. Kotlarchyk and S-H. Chen, J. Chem. Phys. **79**, 2461 (1983).

[38]S.W. Lovesey, *Theory of Neutron Scattering from Condensed Matter Vol.1* (Clarendon, Oxford, 1986), Vol. 1.

[39]J.K. Percus and G.J. Yevick, Phys. Rev. **110**, 1 (1958).

[40]W.L. Griffith, R. Triolo and A.L. Compere, Phys. Rev. A **33**, R2197 (1986).

[41]W.L. Griffith, R. Triolo and A.L. Compere, Phys. Rev. A **35**, 2200 (1987).

[42]S.L. Lee, T. Thomson, F.Y. Ogrin, C. Oates, M. Wismayer, C. Dewhurst, R. Cubitt and S. Harkness, Mat. Res. Symp. Proc. **803,** GG4.4.1 (2004).

[43]T. Thomson, M.F. Toney, S. Raoux, S.L. Lee, S. Sun, C.B. Murray and B.D. Terris J. Appl. Phys. **96**, 1197 (2004).

[44]S. Anders, M.F. Toney, T. Thomson, J.-U. Thiele, B.D.Terris, S. Sun and C.B. Murray, J. Appl. Phys. **93**, 7343 (2003).

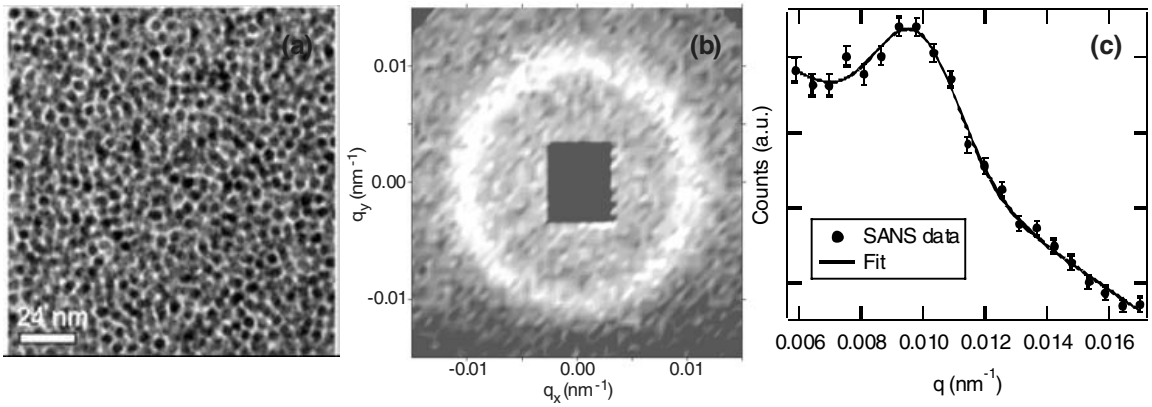

Fig.1: (a) SEM, (b) SANS detector image and (c) integrated SANS signal for a self-assembled unannealed nanoparticle array having a particle diameter of 4nm and a spacing of 6.5nm.

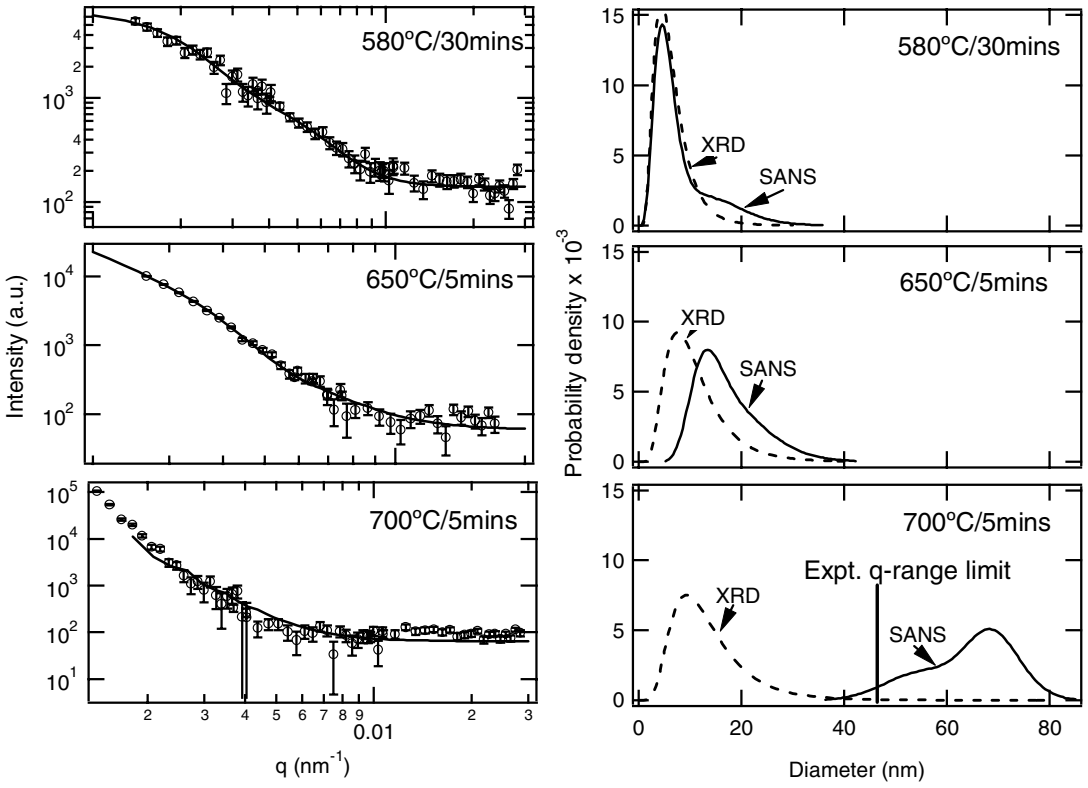

Fig.2: SANS data and simulations (a, b, c) for FePt nanoparticle assemblies for a variety of annealing conditions a) 580°C/30mins b) 650°C/5mins and c) 700°C/5mins. The corresponding particle size distributions obtained from the simulations (solid lines) together with the particle size distribution estimated from XRD data (dashed lines) are shown opposite. Note that the size distribution obtained from the SANS data for the

700°C/5mins annealing condition is subject to greater uncertainty since experimentally the corresponding q range was not completely measured as shown on the figure.

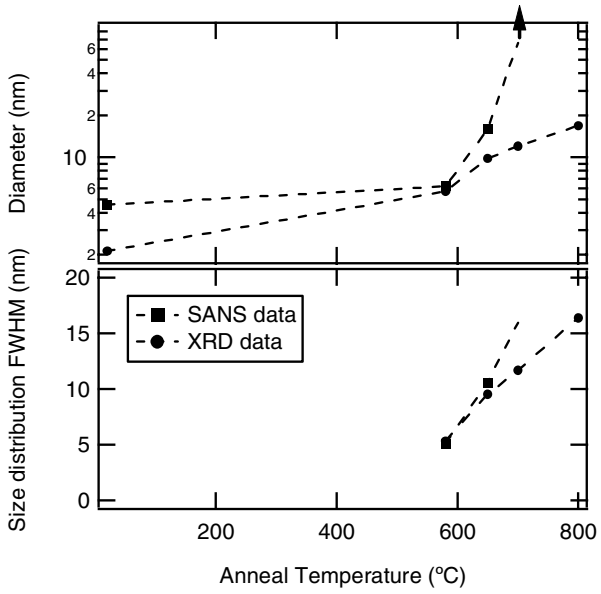

Fig.3: Summary of particle diameters and the full width half maximum (FWHM) of the particle size distributions obtained from SANS and XRD results.

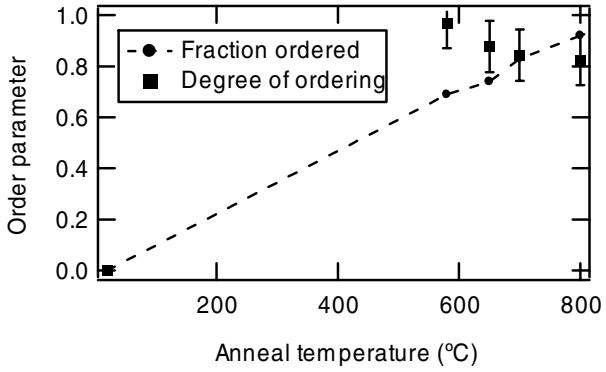

Fig.4: Fraction of particles with $L1_0$ ordering and the degree of ordering within this fraction as a function of anneal temperature. The data show that a two state model, where particles are either not ordered or are essentially fully ordered should be used to describe these nanoparticle arrays. The dotted lines are included as a guide to the eye.